EDGE ARTICLE

CrossMark
click for updates

Structural engineering of porphyrin-based small molecules as donors for efficient organic solar cells†

Hongda Wang,‡[ab] Liangang Xiao,‡[c] Lei Yan,‡[d] Song Chen,‡[a] Xunjin Zhu,*[ab] Xiaobin Peng,*[c] Xingzhu Wang,*[d] Wai-Kwok Wong*[a] and Wai-Yeung Wong*[ab]

Porphyrin-based small molecules as donors have long been ignored in bulky heterojunction organic solar cells due to their unfavorable aggregation and the low charge mobility. With the aim of striking a delicate balance between molecular design, morphology, interfacial layer and device fabrication to maximize the power conversion efficiency (PCE) of organic solar cells, three comparable porphyrin-based small molecules with an acceptor–donor–acceptor configuration have been developed for use as donor materials in solution processed small molecule bulk heterojunction organic solar cells. In these molecules, electron-deficient 3-ethylrhodanine is introduced into the electron-rich porphyrin core through 5,15-bis(phenylethynyl) linkers. Structural engineering with 10,20-bis(2-hexylnonyl) aliphatic peripheral substituent on the porphyrin core, instead of the aromatic substituents such as 10,20-bis[3,5-di(dodecyloxy)phenyl], and 10,20-bis(4-dodecyloxylphenyl), can simultaneously facilitate stronger intermolecular $\pi-\pi$ stacking and higher charge transfer mobility in the film, leading to a maximum PCE of 7.70% in a conventional device. The inverted devices have also been demonstrated to have long-term ambient stability and a comparable PCE of 7.55%.

1. Introduction

Solution processed small molecule (SM) bulk heterojunction organic solar cells (BHJ OSCs) have shown great prospect in the realization of low-cost and large-scale devices due to their characteristics of well-defined structure and molecular weight, and easy synthesis and purification of small molecules.[1,2] Generally, a small molecule as a donor in a solution processed BHJ OSC needs to possess the following features: (i) strong photo-absorption in the visible and near-infrared (NIR) region; (ii) sufficient solubility in solvents; (iii) strong intermolecular interaction in the solid state for efficient charge transfer; and

aInstitute of Molecular Functional Materials, Department of Chemistry and Institute of Advanced Materials, Hong Kong Baptist University, Waterloo Road, Kowloon Tong, Hong Kong, P. R. China. E-mail: xjzhu@hkbu.edu.hk; wkwong@hkbu.edu.hk; rwywong@hkbu.edu.hk
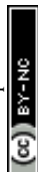
bHKBU Institute of Research and Continuing Education, Shenzhen Virtual University Park, Shenzhen, 518057, P. R. China

cInstitute of Polymer Optoelectronic Materials and Devices, State Key Laboratory of Luminescent Materials and Devices, South China University of Technology, 381 Wushan Road, Guangzhou 510640, P. R. China. E-mail: chxbpeng@scut.edu.cn

dKey Laboratory of Advanced Functional Polymer Materials of Colleges and Universities of Hunan Province and Key Lab of Environment-friendly Chemistry and Application in Ministry of Education, College of Chemistry, Xiangtan University, Xiangtan 411105, Hunan Province, China. E-mail: xzwang@xtu.edu.cn

† Electronic supplementary information (ESI) available. See DOI: 10.1039/c5sc04783h

‡ H. W., L. X., L. Y. and S. C. contribute equally to this work.

(iv) excellent film formation ability. In the search for appropriate small molecule donors, various frameworks have been examined, including benzo[1,2-b:4,5-b′]dithiophene (BDT),[3,4] boron dipyrromethene,[5,6] diketopyrrolopyrrole,[7–9] phthalocyanine,[10] merocyanine,[11] and squaraine.[12–14] Over the past decade, the power conversion efficiencies (PCEs) of the solution processed SM BHJ OSCs have steadily improved. Since Bazan and Heeger *et al.* first reported a PCE of 6.7% based on a small molecule donor with 3,3′-di-2-ethylhexylsilylene as the central building block,[15] the PCE was steadily enhanced to 9.02% by the structural optimization of both small molecules and devices in BHJ OSCs.[16,17] Chen *et al.* also reported a series of small molecules with an oligothiophene unit as the core unit, and the efficiency was also over 9% after the optimization of the molecular structure.[18,19] On the other hand, porphyrins and their analogues exhibit some intrinsic features that are attractive for their application in photovoltaics.[20] They have strong absorption with high extinction coefficients (ε) in both the blue (Soret band) and red (Q-band) regions, and their photo- and electrochemistry can readily be adjusted through peripheral functionalization and by varying of the metal center. It is known that "push–pull" porphyrin derivatives have been successfully applied in dye-sensitized solar cells.[21–23] However, discouraging PCEs were obtained when employing porphyrins and their analogues as donor materials in BHJ devices. Very recently, Peng and co-workers used {5,15-bis[3,5-di(dodecyloxy)phenyl] porphyrinato}zinc(ii) and 2,1,3-benzothiadiazole (BTD) to

construct donor–acceptor–donor (A–D–A) small molecules as donors in BHJ OSCs. Since the two bulky 3,5-di(dodecyloxyl) phenyl substituents that are almost perpendicular to the porphyrin core suppress the intermolecular π–π stacking, a relatively poor photovoltaic performance was achieved.[24]

Subsequently, they employed less bulky *meso*-substituents such as 4-octyloxy-phenyl and 5-(2-ethylhexyl)-thienyl in the new A–D–A porphyrin-cored molecules, which can exhibit stronger intermolecular π–π stacking in the solid state, leading to a higher hole mobility and better photovoltaic performance.[25,26] It is obvious that the *meso*-phenyl substitutions with an almost orthogonal orientation relative to the porphyrin plane significantly prevent the intermolecular π–π stacking, as well as intermolecular charge transport.[27] Our recent work further demonstrated that the direct peripheral *meso*-alkyl substitutions on the porphyrin ring could not only improve the solubility of small molecules in most organic solvents, but also control the film morphology and crystallinity, leading to an enhancement of charge transport.[28]

To rigorously evaluate the effect of peripheral aromatic or aliphatic *meso*-substituents of the porphyrin ring on the light harvesting, solubility, morphology, exciton diffusion and dissociation, charge transport and collection, and ultimate PCE, three A–D–A structural type porphyrin-based small molecules were carefully designed and prepared. Typically, 3-ethylrhodanine as the terminal unit bridged by a phenylethynyl moiety with porphyrins {5,15-bis[3,5-di(dodecyloxyl)phenyl]-porphyrinato} zinc(Ⅱ), [5,15-bis(4-dodecyloxylphenyl)-porphyrinato]zinc(Ⅱ), and [5,15-bis(2-hexylnonyl)-porphyrinato]zinc(Ⅱ), afforded **4a**, **4b** and **4c**, respectively (Scheme 1). Subsequently, their photovoltaic performances as donors were investigated systematically in conventional devices with a configuration of ITO/PEDOT:PSS/ SM:PC$_{71}$BM/PFN/Al (where PFN is poly[[(9,9-bis(3′-(N,N-dimethylamino)-propyl)-2,7-fluorene)-*alt*-2,7-(9,9-dioctylfluorene)]]). Inverted devices of ITO/Ca/SM:PC$_{71}$BM/MoO$_3$/Ag were also fabricated and tested in the following studies.

2. Results and discussion

2.1 Synthesis and characterization

The synthetic route for **4a–c** is shown in Scheme 1. It should be noted that the use of the zinc porphyrin complex instead of
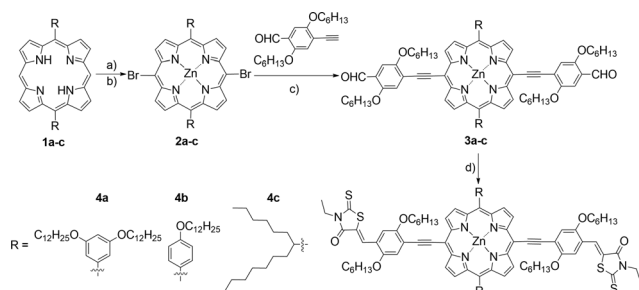
a porphyrin free base is necessary, due to the higher stability of the metal complex and it also helps to improve the photovoltaic properties of the OSC devices.[26] The Sonogashira coupling of **2a–c** with 4-ethynyl-2,5-bis(hexyloxy)benzaldehyde produced the porphyrin intermediates **3a–c** in good yields. The target compounds **4a–c** were prepared by the Knoevenagel condensation of 3-ethylrhodanine with **3a–c**, respectively. Although the solubility of **4a** and **4b** is not as good as **4c** in organic solvents such as chloroform, THF, and toluene, all three π-conjugated small molecules could be readily processed in solution to form smooth and pinhole-free films using spin-coating technology.

2.2 Optical and electrochemical properties

The normalized UV-vis absorption spectra of **4a–c** in CH$_2$Cl$_2$ solutions and spin-casted thin films are depicted in Fig. 1, and the relevant optical data including the wavelengths of the absorption maxima (λ_{max}), molar extinction coefficients, absorption edge wavelengths (λ_{onset}), and optical band gaps (E_g^{opt}) are summarized in Table 1. As shown in Fig. 1, **4a** in dilute CH$_2$Cl$_2$ solution shows a Soret band at 504 nm with a molar extinction coefficient (ε) of 1.55×10^5 M^{-1} cm^{-1} and a Q band at 682 nm with a molar extinction of 1.39×10^5 M^{-1} cm^{-1}. Additionally, **4b** in CH$_2$Cl$_2$ solution presents a similar Soret band at 505 nm with a ε of 1.61×10^5 M^{-1} cm^{-1} and a bathochromically shifted Q band at 720 nm with a ε of 1.53×10^5 M^{-1} cm^{-1}. As for *meso*-2-hexylnonyl substituted **4c**, a Soret band at 502 nm with a ε of 1.95×10^5 M^{-1} cm^{-1} and a Q band at 696 nm with a ε of 1.87×10^5 M^{-1} cm^{-1} were observed. Apparently, **4c** exhibits much stronger absorption at both Soret and Q bands than **4a** and **4b**.

There is no significant changes in Soret bands due to minor electronic perturbations between the porphyrin ring and either *meso*-aliphatic or aromatic substituents.[29] In comparison with
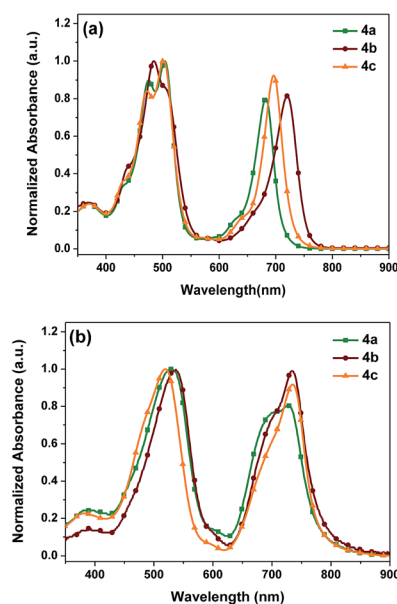

Scheme 1 Synthetic route for **4a–c**. Reaction conditions: (a) NBS, CH$_2$Cl$_2$, pyridine, 0 °C; (b) Zn(AcO)$_2$, CHCl$_3$, reflux, 4 h; (c) Pd(PPh$_3$)$_4$, CuI, Et$_3$N, THF, 50 °C, overnight; (d) 3-ethylrhodanine, CHCl$_3$, piperidine, reflux, overnight.

Fig. 1 UV-visible-NIR absorption spectra of **4a–c** in CH$_2$Cl$_2$ solution (a) and films (b).

Table 1 Optical and electrochemical data for **4a–c**

Comp.	λ_{max}/nm (CH_2Cl_2) ($\varepsilon/10^5$ M^{-1} cm^{-1})	λ_{max}/nm (film)	λ_{onset}/nm (film)	$E_{ox}{}^a$ [V]	$E_{HOMO}{}^a$ [eV]	E_{LUMO} [eV]	E_g^{optb} [eV]
4a	475 (1.55), 504 (1.73), 683 (1.39)	537, 733	779	0.49	−5.19	−3.59	1.60
4b	484 (1.61), 505 (1.61), 720 (1.53)	526, 726	790	0.45	−5.15	−3.60	1.55
4c	472 (1.64), 502 (1.95), 696 (1.81)	520, 735	780	0.42	−5.12	−3.52	1.60

[a] HOMO levels were measured in DCM with 0.1 M tetrabutylammonium hexafluorophosphate (TBAPF) calibrated with ferrocene/ferrocenium (Fc/Fc$^+$) as an external reference. [b] The HOMO and LUMO levels were estimated by the following equation: HOMO = $-(4.70 + E_{ox})$, LUMO = HOMO − E_g^{Opt}. Optical band gap estimated from the formula of $1240/\lambda_{onset}$, λ_{onset} is the absorption onset of the film spectrum.

4a, the absorption maxima of the Q bands in **4b** and **4c** exhibit a significant red-shift of 38 and 14 nm, respectively, which indicates a stronger intramolecular charge transfer (ICT) between the donor and acceptor units in **4b** and **4c**. On the other side, their absorption maxima for both the Soret and Q bands in the thin films were significantly red-shifted, which indicates that a strong π–π intermolecular interaction exists in the solid state due to the optically active J-aggregation.[30]

Cyclic voltammetry (CV) was performed to investigate the electrochemical properties of **4a–c** and the electrochemical data are shown in Table 1. The HOMO energy levels of **4a–c** were calculated to be −5.19, −5.15 and −5.12 eV, respectively. Furthermore, the optical band gaps (E_g) for **4a–c** were estimated from the absorption spectra in the films with values of 1.60, 1.55 and 1.60 eV, respectively. Therefore the potential levels of the LUMO for **4a–c** were obtained from LUMO = HOMO − E_g, with values of −3.59, −3.60 and −3.52 eV, respectively. The HOMO levels of **4a–c** are located within the band gap of PC$_{61}$BM, while the LUMO levels are sufficiently higher (around −3.5 eV) than that of PC$_{61}$BM (−4.0 eV). The results indicate that **4a–c** are compatible with the commonly used acceptor material PC$_{61}$BM or PC$_{71}$BM in BHJ OSCs.

2.3 Photovoltaic properties

Subsequently, BHJ OSCs using **4a–c** as donor materials were fabricated and tested under AM1.5 illumination, 100 mW cm^{-2} in a device structure of ITO/PEDOT:PSS/SM:PC$_{61}$BM (or PC$_{71}$BM)/PFN/Al. Following the conventional practice for fabricating solution processed SM BHJ OSCs, the active layers were spin-coated from their chlorobenzene solutions with 1 vol% pyridine as an additive and a film thickness of approximately 80 nm was obtained. The optimized J–V curves are reported in Fig. 2a, and the photovoltaic performances are summarized in Table 2. With the optimized weight ratio of **4a** to PC$_{61}$BM at 1 : 1, the best but low PCE of 1.42% was obtained, together with a short circuit current (J_{SC}) of 6.44 mA cm^{-2}, an open-circuit voltage (V_{OC}) of 0.76 V, and a fill factor (FF) of 28.9%. The optimized weight ratio of **4b** to PC$_{61}$BM was also found to be 1 : 1, yielding a moderate PCE of 4.55% with V_{OC} of 0.80 V, J_{SC} of 10.09 mA cm^{-2} and FF of 56.3%. In contrast, the device based on **4c**/PC$_{61}$BM (1 : 1, w/w) received an impressive PCE of 4.98%, with a V_{OC} of 0.89 V, a FF of 52.1%, and a significantly higher J_{SC} of 10.72 mA cm^{-2} due to its good solubility, high light harvesting properties and strong π–π stacking intermolecular interaction.

To further optimize their photovoltaic performance in BHJ OSCs, PC$_{71}$BM was used as the electron acceptor for its higher absorption coefficient in the visible range. As expected, the active layers based on **4a–c**/PC$_{71}$BM (1 : 1, w/w) yielded improved device performances with PCEs of 3.21%, 5.07% and 5.20%, and J_{SC} of 7.2, 10.14, and 12.14 mA cm^{-2} for **4a**, **4b** and **4c** (Table 2), respectively. Specifically, the devices with PC$_{71}$BM as the acceptor exhibit an exceptionally higher V_{OC} of 0.90 V, 0.90 V and 0.89 V for **4a**, **4b** and **4c**, respectively. It's not surprising that the morphologies and thus performance of state-of-the-art donor small molecules are sensitive to the choice of fullerene. Peng and co-workers reported that devices based on DPP-porphyrin small molecules performed better with PC$_{61}$BM as the acceptor rather than PC$_{71}$BM.[24–26] The possible reason is that the solubility of PC$_{71}$BM in some organic solvents is not as good as that of PC$_{61}$BM, which leads to an unfavorable morphology and deteriorates the performance of OSCs.[31,32] During the device optimization, it was found that the performance of the cells based on **4c** could be further improved by reducing the annealing time. When the annealing time is 5 min, the device yielded an impressive PCE of 6.11%, with a J_{SC} of

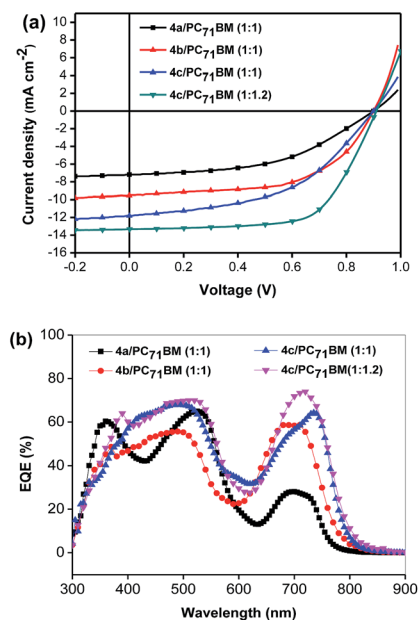**Fig. 2** The best J–V curves (a) and EQEs (b) of devices based on **4a–c**/PC$_{71}$BM.

Table 2 Solar cell characteristics of the optimized solar cells based on **4a–c**/PC$_{71}$BM (or PC$_{61}$BM)

Device	Additive	Annealing time at 90 °C (min)	J_{SC} (mA cm^{-2})	V_{OC} (V)	FF (%)	PCE (%)
4a/PC$_{61}$BM[a]	1% pyridine	10	6.44	0.76	28.98	1.42
4a/PC$_{71}$BM[a]	1% pyridine	10	7.20	0.90	48.12	3.21
4b/PC$_{61}$BM[a]	1% pyridine	10	10.09	0.80	56.33	4.55
4b/PC$_{71}$BM[a]	1% pyridine	10	10.14	0.90	55.60	5.07
4c/PC$_{61}$BM[a]	1% pyridine	10	10.72	0.89	52.12	4.98
4c/PC$_{71}$BM[a]	1% pyridine	10	12.14	0.89	48.07	5.20
4c/PC$_{71}$BM[a]	1% pyridine	0	4.84	0.92	29.18	1.30
4c/PC$_{71}$BM[a]	1% pyridine	5	12.28	0.91	54.67	6.11
4c/PC$_{71}$BM[a]	1% pyridine	20	12.22	0.90	50.35	5.54
4c/PC$_{71}$BM[b]	1% pyridine	5	13.32	0.91	63.60	7.70
4c/PC$_{71}$BM[c]	1% pyridine	0	6.26	0.892	38.1	2.12
4c/PC$_{71}$BM[c]	1% pyridine	5	12.89	0.901	65.1	7.55
4c/PC$_{71}$BM[d]	1% pyridine	—	12.87	0.910	64.5	7.55
4c/PC$_{71}$BM[e]	1% pyridine	—	12.87	0.882	59.2	6.62
4c/PC$_{71}$BM[f]	1% pyridine	—	12.53	0.876	57.0	6.26

[a] **4a–c**/PC$_{61}$BM or **4a–c**/PC$_{71}$BM with a 1 : 1 weight ratio in solar cells with conventional structures based on fresh cells. [b] **4c**/PC$_{71}$BM with a 1 : 1.2 weight ratio in solar cells with conventional structures based on fresh cells. [c] **4c**/PC$_{71}$BM with a 1 : 1.2 weight ratio in solar cells with inverted structures based on fresh cells. [d] **4c**/PC$_{71}$BM with a 1 : 1.2 weight ratio in solar cells with inverted structures with encapsulation based on aging for 3 days. [e] **4c**/PC$_{71}$BM with a 1 : 1.2 weight ratio in solar cells with inverted structures with encapsulation based on aging for 10 days. [f] **4c**/PC$_{71}$BM with a 1 : 1.2 weight ratio in solar cells with inverted structures with encapsulation based on based on aging for 30 days.

12.28 mA cm^{-2}, a V_{OC} of 0.91 V, and a FF of 54.6%. Since **4c** shows a much better solubility than **4a** or **4b** in organic solvent, the weight ratio of **4c** to PC$_{61}$BM was further optimized to be 1 : 1.2, yielding the highest PCE of 7.70% with a V_{OC} of 0.91 V, a J_{SC} of 13.32 mA cm^{-2} and a FF of 63.6%. In general, the energy loss (E_{loss}), which connects E_g and V_{OC} together and is defined as $E_{loss} = E_g - eV_{OC}$, is one of the most important parameters to evaluate solar cells. In this study, an exceptionally high V_{OC} of 0.91 V was obtained for the optimized cell based on **4c**, in spite of a high energy loss of 0.69 eV. By comparison, Peng and his co-workers reported a DPP-porphyrin small molecule with a very low energy band gap of 1.37 eV and an open circuit voltage of 0.78 V obtained in BHJ OSCs, corresponding to a very low energy loss of 0.59 eV.[26]

The external quantum efficiency (EQE) spectra of the optimized devices based on **4a–c** are shown in Fig. 2b. The EQE curve of **4c**/PC$_{71}$BM (w/w, 1 : 1.2) with 1% pyridine exhibits efficient photo-electron conversion efficiency from 400 to 800 nm, with the highest EQE value reaching 73% at 735 nm. The calculated J_{SC} integrated from the EQE for **4c** is 13.32 mA cm^{-2} shows a mismatch of about 5% compared to the J_{SC} from the J–V measurement. In comparison, the EQE values of the devices based on **4a** or **4b** are below 50% in the range of 620–800 nm, resulting in lower J_{SC} values. This is also consistent with the weaker absorptions of **4a** and **4b** in solution, as compared to **4c**. Definitely, the incorporation of the alkyl side chains could indeed improve significantly the photo-electron conversion efficiency.

To circumvent the degradation problem in the conventional structure, the inverted structure has been intensively investigated in polymer-based BHJ solar cells.[33–37] Very recently, some SMs have also been explored and have performed well in inverted device architectures.[38–42] Hence, an inverted architecture of ITO/Ca/SM:PC$_{71}$BM/MoO$_3$/Ag has been applied to **4c**,

which yielded a PCE of 7.55%, corresponding to a J_{SC} of 12.89 mA cm^{-2}, a V_{OC} of 0.91 V, and a FF of 65.1% under the optimized conditions (Fig. 3 and Table 2). It should be noted that the inverted photovoltaic devices were processed and characterized under ambient atmosphere (see ESI†). Although the inverted structure shows a comparable performance to that of the conventional one, the former exhibits impressive stability with the same PCE of 7.55% measured after 3 days of storage in air and retains 83% of the original value even after storage in air for 30 days.
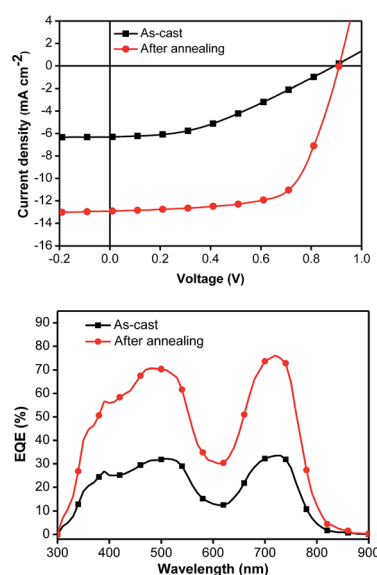

Fig. 3 The J–V curves (top) and EQE plots (bottom) of the inverted devices with **4c**/PC$_{71}$BM (1 : 1.2, w/w) as-cast (black line) and after annealing for 5 minutes at 90 °C (red line).

2.4 Morphology and mobility

To understand the effect of different peripheral substitutions on the porphyrin ring, the morphology of the active layers of **4a**–**c**/PC₇₁BM (1 : 1, w/w%) was investigated by tapping-mode atomic force microscope (AFM). Additionally, height and phase images were taken from the blend films as shown in Fig. 4. It should be noted that the blend films of **4a**–**c**/PC₇₁BM were prepared with 1% pyridine as an additive, using a procedure identical to that for the active layers in the devices. The values of root-means-square (RMS) roughness are 0.852, 0.780 and 0.567 nm for the blend films **4a**–**c**/PC₇₁BM, respectively. The lowest RMS roughness of **4c**/PC₇₁BM indicates that **4c** has the best miscibility with PC₇₁BM and may form a finer interpenetrating network to facilitate both exciton separation and charge transport. As expected, the blend film of **4c**/PC₇₁BM exhibits a better donor/acceptor interpenetrating network with much smaller phase separation domains (Fig. 4f), which is beneficial for efficient exciton dissociation and charge transporting, and should lead to an increased J_{SC} and FF in BHJ OSCs.[43,44] In contrast, surface relief and a larger domain size were observed for the **4a**/PC₇₁BM and **4b**/PC₇₁BM films, which indicates the poor film-forming characteristics due to the perpendicular aromatic peripheral substitutions on the porphyrin ring. Without a doubt, the unique characteristics of 10,20-bis(5,15-alkyl) substituted porphyrin are expected to form blend films possessing more efficient intermolecular π–π stacking and more suitable surface morphology for BHJ OSCs.

As shown in Fig. 5, the phase and height images were taken from the blend films of **4c**/PC₇₁BM (1 : 1.2, w/w%) in inverted devices as-casted and after annealing at 90 °C for 5 minutes. The values of the root-means-square (RMS) roughness are 4.48 and 0.88 nm for the blend films **4c**/PC₇₁BM, as-cast and after annealing, respectively. Without a doubt, annealing at an appropriate temperature is necessary for the formation of high quality films with nanoscale amorphous domains that produce efficient charge separation and improved solar cell performances.

Since the values of J_{SC} and FF are generally reflected by the charge transport properties of the photoactive film, the hole mobilities of the porphyrin/fullerene blend films were measured for a device configuration of ITO/PEDOT:PSS/active
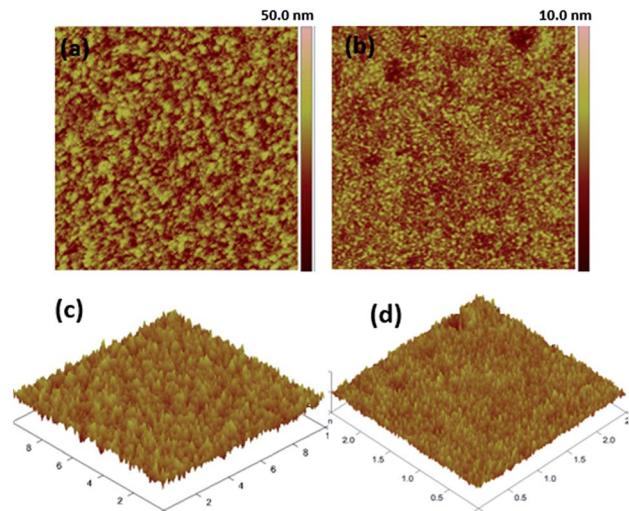

Fig. 5 Tapping mode AFM phase images (a and b) and height (c and d) of **4c**/PC₇₁BM (1 : 1.2, w/w%) in the inverted devices.

layer/MoO₃/Al, and were estimated using the space charge limited current (SCLC) model. The J–V characteristics of the polymers and the porphyrin/PC₇₁BM blend films are shown in Fig. S1.† The hole mobilities of the **4a**–**c**/PC₇₁BM blend films were determined to be 1.57×10^{-5} cm² V⁻¹ s⁻¹ (**4a**), 8.48×10^{-5} cm² V⁻¹ s⁻¹ (**4b**), and 2.18×10^{-4} cm² V⁻¹ s⁻¹ (**4c**). Obviously, all the **4a**–**c**/PC₇₁BM blend films show reasonably high hole mobilities appropriate for photovoltaic devices. Notably, the device based on **4c**/PC₇₁BM exhibits the highest mobility of about one order of magnitude higher than that based on **4a**/PC₇₁BM. This is consistent with the highest J_{SC} values of 13.32 mA cm⁻² and the best photovoltaic performance based on the active layer of **4c**/PC₇₁BM (1 : 1.2, w/w%). Without a doubt, the enhanced charge transport property is ascribed to the stronger intermolecular π–π stacking interaction and better surface morphology of the blend film of 5,15-dialkylated porphyrin-cored small molecule.[45] At the same time, ultraviolet photoelectron spectroscopy (Fig. S2†) shows that the work functions of the annealed layer of ITO/PEDOT:PSS/**4a**–**c**:PC₇₁BM decrease gradually from 3.75 eV for **4a**, 3.66 eV for **4b**, to 3.44 eV for **4c**, which also accounts for the device efficiency improvement with the increasing J_{SC} from 7.20 mA cm⁻² for **4a** and 10.14 mA cm⁻² for **4b**, to 12.14 mA cm⁻² for **4c** (Table 2).[46]

3. Conclusion

In summary, three new porphyrin-based small molecules **4a**–**c** were prepared, in which 3-ethylrhodanine as a terminal electron deficient unit was introduced into aromatic and aliphatic 10,20-*meso*-substituted porphyrin rings as the central building block *via* the 5,15-*meso*-phenylethynyl linker. Although the aliphatic 10,20-bis(2-hexylnonyl) substitution in **4c** has little influence on the optical absorption in solution, it significantly changes the optical and crystallization properties of the films. Based on **4c**/PC₇₁BM (1 : 1.2, w/w%) which has stronger intermolecular π–π stacking and more suitable surface morphology, the device possesses a much higher J_{SC}, corresponding to the highest PCE

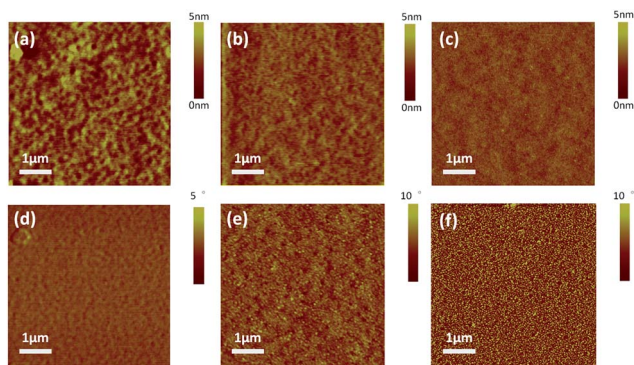Fig. 4 Tapping mode AFM height (a–c) and phase images (d–f) of **4a**/PC₇₁BM, **4b**/PC₇₁BM, and **4c**/PC₇₁BM blend films of the best devices.

of 7.70%. Moreover, the inverted structure based on **4c**/PC$_{71}$BM (1 : 1.2, w/w%) shows a comparable performance to that of the conventional one, and its stability was also investigated revealing the same PCE of 7.55% measured after 3 days of storage and retaining 83% of the original value even after storage in air for 30 days. The primary results demonstrate that porphyrin derivatives can play a more important role as donors in BHJ OSCs by the judicious optimization of their molecular structures and careful device engineering.

4. Experimental section

4.1 Materials and methods

3,5-Di(dodecyloxy)benzaldehyde, 4-octyloxybenzaldehyde, 2-hexyldecanal and 1,4-dibromo-2,5-bis(hexyloxy)benzaldehyde were prepared according to the literature procedures, and characterized by comparing their ^{1}H NMR and ^{13}C NMR spectra with those found in the literature.[47] [6,6]-Phenyl-C$_{71}$-butyric acid methyl ester (PC$_{71}$BM) was purchased from Nano-C. All other reagents were used as received without further purification, unless stated otherwise.

4.2 General procedure for the preparation of 4a–c

To a solution of **3a–c** (0.137 mmol) in CHCl$_3$ (20 mL), two drops of piperidine and 3-ethylrhodanine (228.3 mg, 1.370 mmol) were added, and the resulting solution was refluxed for 12 h under argon. The reaction was quenched with water (30 mL) and extracted with CHCl$_3$ (3 × 20 mL). The organic layer was dried over Na$_2$SO$_4$ and evaporated to dryness. The solid residue was purified first on a silica gel column and second by preparative thin layer chromatography using a CHCl$_3$ as the eluent. Further recrystallization from hexane and CHCl$_3$ mixed solvent five times afforded the target compounds **4a–c** as a black solid.

4a. 170.2 mg, 56% yield. ^{1}H NMR (400 MHz, CDCl$_3$, δ): 0.72–0.77 (m, 18H, CH$_3$), 0.86–0.89 (m, 6H, CH$_3$), 1.15–1.42 (m, 92H, CH$_2$), 1.44–1.51 (m, 4H), 1.69–1.87 (m, 16H), 2.08–2.14 (m, 4H), 4.05–4.17 (m, 20H), 6.84 (s, 2H), 6.88 (s, 2H), 7.29 (s, 4H), 7.33 (s, 2H), 8.12 (s, 2H), 8.88 (d, J = 4.4 Hz, 2H, β-pyrrolic H), 9.65 (d, J = 4.8 Hz, 4H, β-pyrrolic H). MALDI-TOF (m/z): [M + H]$^+$ calcd for C$_{132}$H$_{182}$N$_6$O$_{10}$S$_4$Zn, 2206.5417; found, 2206.5417.

4b. 144.5 mg, 57% yield. ^{1}H NMR (400 MHz, CDCl$_3$ δ): 0.86–0.95 (m, 18H, CH$_3$), 1.20–1.24 (m, 6H, CH$_2$), 1.31–1.46 (m, 40H, CH$_2$), 1.48–1.52 (m, 12H), 1.65–1.67 (m, 4H), 1.76–1.78 (m, 4H), 1.85–1.89 (m, 4H), 1.99–2.02 (m, 4H), 2.24–2.26 (m, 4H), 4.14–4.16 (m, 4H), 4.20–4.26 (m, 8H), 4.33–4.36 (m, 4H), 7.16 (s, 2H), 7.46 (d, J = 8.4 Hz, 4H), 7.91 (s, 2H), 8.34 (d, J = 8.4 Hz, 4H), 8.44 (s, 2H), 9.22 (d, J = 4.4 Hz, 2H, β-pyrrolic H), 10.26 (d, J = 4.8 Hz, 4H, β-pyrrolic H). MALDI-TOF (m/z): [M + H]$^+$ calcd for C$_{108}$H$_{134}$N$_6$O$_8$S$_4$Zn, 1837.9050; found, 1837.9050.

4c. 154.7 mg, 65% yield. ^{1}H NMR (400 MHz, CDCl$_3$, δ): 0.68–0.73 (m, 12H, CH$_3$), 0.90–1.03 (m, 46H), 1.23–1.33 (m, 12H), 1.44 (m, 12H), 1.61 (m, 8H), 1.86–1.99 (m, 8H), 2.33 (m, 4H), 2.71 (m, 4H), 2.93 (m, 4H), 4.23 (m, 8H), 4.35 (d, J = 5.6 Hz, 4H), 5.15 (m, 2H), 7.08 (d, J = 6.0 Hz, 2H), 7.44 (m, 2H), 8.28 (d, J = 4.4 Hz, 2H), 9.54 (d, 2H), 9.62 (d, 2H), 9.82 (m, 4H). MALDI-TOF (m/z): [M + H]$^+$ calcd for C$_{102}$H$_{138}$N$_6$O$_6$S$_4$Zn, 1737.8737; found, 1736.8991.

References

1 Y. Li, *Acc. Chem. Res.*, 2012, **45**, 723.
2 Y. Lin, Y. Li and X. Zhan, *Chem. Soc. Rev.*, 2012, **41**, 4245.
3 J. Zhou, Y. Zuo, X. Wan, G. Long, Q. Zhang, W. Ni, Y. Liu, Z. Li, G. He and C. Li, *J. Am. Chem. Soc.*, 2013, **135**, 8484.
4 Y. Liu, C.-C. Chen, Z. Hong, J. Gao, Y. M. Yang, H. Zhou, L. Dou, G. Li and Y. Yang, *Sci. Rep.*, 2013, **3**, 3356.
5 W. Liu, A. Tang, J. Chen, Y. Wu, C. Zhan and J. Yao, *ACS Appl. Mater. Interfaces*, 2014, **6**, 22496.
6 L. Xiao, H. Wang, K. Gao, L. Li, C. Liu, X. Peng, W.-Y. Wong, W.-K. Wong and X. Zhu, *Chem.–Asian J.*, 2015, **10**, 1513.
7 Y. Lin, L. Ma, Y. Li, Y. Liu, D. Zhu and X. Zhan, *Adv. Energy Mater.*, 2013, **3**, 1166.
8 J. Liu, Y. Sun, P. Moonsin, M. Kuik, C. M. Proctor, J. Lin, B. B. Hsu, V. Promarak, A. J. Heeger and T. Q. Nguyen, *Adv. Mater.*, 2013, **25**, 5898.
9 J. Yuan, L. Xiao, B. Liu, Y. Li, Y. He, C. Pan and Y. Zou, *J. Mater. Chem. A*, 2013, **1**, 10639.
10 E. W. Snedden, A. P. Monkman and F. B. Dias, *Adv. Mater.*, 2013, **25**, 1930.
11 A. Zitzler-Kunkel, M. R. Lenze, N. M. Kronenberg, A.-M. Krause, M. Stolte, K. Meerholz and F. Würthner, *Chem. Mater.*, 2014, **26**, 4856.
12 F. Silvestri, M. D. Irwin, L. Beverina, A. Facchetti, G. A. Pagani and T. J. Marks, *J. Am. Chem. Soc.*, 2008, **130**, 17640.
13 Y. Chen, Y. Zhu, D. Yang, Q. Luo, L. Yang, Y. Huang, S. Zhao and Z. Lu, *Chem. Commun.*, 2015, **51**, 6133.
14 F. Silvestri, M. D. Irwin, L. Beverina, A. Facchetti, G. A. Pagani and T. J. Marks, *J. Am. Chem. Soc.*, 2008, **130**, 17640.
15 Y. Sun, G. C. Welch, W. L. Leong, C. J. Takacs, G. C. Bazan and A. J. Heeger, *Nat. Mater.*, 2012, **11**, 44.
16 T. S. van der Poll, J. A. Love, T.-Q. Nguyen and G. C. Bazan, *Adv. Mater.*, 2012, **24**, 3646.
17 V. Gupta, A. K. K. Kyaw, D. H. Wang, S. Chand, G. C. Bazan and A. J. Heeger, *Sci. Rep.*, 2013, **3**, 1965.

18 B. Kan, M. Li, Q. Zhang, F. Liu, X. Wan, Y. Wang, W. Ni, G. Long, X. Yang, H. Feng, Y. Zuo, M. Zhang, F. Huang, Y. Cao, T. P. Russell and Y. Chen, *J. Am. Chem. Soc.*, 2015, **137**, 3886.

19 Q. Zhang, B. Kan, F. Liu, G. Long, X. Wan, X. Chen, Y. Zuo, W. Ni, H. Zhang, M. Li, Z. Hu, F. Huang, Y. Cao, Z. Liang, M. Zhang, T. P. Russell and Y. Chen, *Nat. Photonics*, 2014, **9**, 35.

20 J. Kesters, P. Verstappen, M. Kelchtermans, L. Lutsen, D. Vanderzande and W. Maes, *Adv. Energy Mater.*, 2015, **5**, 1500218.

21 M. Urbani, M. Grätzel, M. K. Nazeeruddin and T. s. Torres, *Chem. Rev.*, 2014, **114**, 12330.

22 S. Mathew, A. Yella, P. Gao, R. Humphry-Baker, B. F. Curchod, N. Ashari-Astani, I. Tavernelli, U. Rothlisberger, M. K. Nazeeruddin and M. Grätzel, *Nat. Chem.*, 2014, **6**, 242.

23 A. Yella, H.-W. Lee, H. N. Tsao, C. Yi, A. K. Chandiran, M. K. Nazeeruddin, E. W. G. Diau, C.-Y. Yeh, S. M. Zakeeruddin and M. Grätzel, *Science*, 2011, **334**, 629.

24 L. Li, Y. Huang, J. Peng, Y. Cao and X. Peng, *J. Mater. Chem. A*, 2013, **1**, 2144.

25 H. Qin, L. Li, F. Guo, S. Su, J. Peng, Y. Cao and X. Peng, *Energy Environ. Sci.*, 2014, **7**, 1397.

26 K. Gao, L. Li, T. Lai, L. Xiao, Y. Huang, F. Huang, J. Peng, Y. Cao, F. Liu, T. P. Russell, R. A. J. Janssen and X. Peng, *J. Am. Chem. Soc.*, 2015, **137**, 7282.

27 T. S. Balaban, A. Eichhöfer and J. M. Lehn, *Eur. J. Org. Chem.*, 2000, **21**, 4047.

28 S. Chen, L. Xiao, X. Zhu, X. Peng, W.-K. Wong and W.-Y. Wong, *Chem. Commun.*, 2015, **51**, 14439.

29 P. Thamyongkit, M. Speckbacher, J. R. Diers, H. L. Kee, C. Kirmaier, D. Holten, D. F. Bocian and J. S. Lindsey, *J. Org. Chem.*, 2004, **69**, 3700.

30 Y. Ren, A. M. Hiszpanski, L. Whittaker-Brooks and Y.-L. Loo, *ACS Appl. Mater. Interfaces*, 2014, **6**, 14533.

31 Z. Ma, E. Wang, K. Vandewal, M. R. Andersson and F. Zhang, *Appl. Phys. Lett.*, 2011, **99**, 143302.

32 M. Williams, N. R. Tummala, S. G. Aziz, C. Risko and J.-L. Brédas, *J. Phys. Chem. Lett.*, 2014, **5**, 3427.

33 Y. Sun, J. H. Seo, C. J. Takacs, J. Seifter and A. J. Heeger, *Adv. Mater.*, 2011, **23**, 1679.

34 Z. He, C. Zhong, S. Su, M. Xu, H. Wu and Y. Cao, *Nat. Photonics*, 2012, **6**, 591.

35 C. E. Small, S. Chen, J. Subbiah, C. M. Amb, S.-W. Tsang, T.-H. Lai, J. R. Reynolds and F. So, *Nat. Photonics*, 2012, **6**, 115.

36 S.-H. Liao, H.-J. Jhuo, Y.-S. Cheng and S.-A. Chen, *Adv. Mater.*, 2013, **25**, 4766.

37 A. R. B. M. Yusoff, D. Kim, H. P. Kim, F. K. Shneider, W. J. da Silva and J. Jang, *Energy Environ. Sci.*, 2015, **8**, 303.

38 X. Tong, B. E. Lassiter and S. R. Forrest, *Org. Electron.*, 2010, **11**, 705.

39 F. J. Zhang, D. W. Zhao, Z. L. Zhuo, H. Wang, Z. Xu and Y. S. Wang, *Sol. Energy Mater. Sol. Cells*, 2010, **94**, 2416.

40 A. K. K. Kyaw, D. H. Wang, V. Gupta, J. Zhang, S. Chand, G. C. Bazan and A. J. Heeger, *Adv. Mater.*, 2013, **25**, 2397.

41 D. Y. Liu, F. Qu, X. N. Zhao and J. M. You, *J. Phys. Chem. C*, 2015, **119**, 17979.

42 G. Long, B. Wu, X. Yang, B. Kan, Y.-c. Zhou, L.-c. Chen, X. Wan, H.-l. Zhang, T. C. Sum and Y. Chen, *ACS Appl. Mater. Interfaces*, 2015, **7**, 21245.

43 W. L. Leong, G. C. Welch, J. Seifter, J. H. Seo, G. C. Bazan and A. J. Heeger, *Adv. Energy Mater.*, 2013, **3**, 356.

44 M. S. Su, C. Y. Kuo, M. C. Yuan, U. Jeng, C. J. Su and K. H. Wei, *Adv. Mater.*, 2011, **23**, 3315.

45 L. Zhou, Z.-X. Xu, Y. Zhou, Y. Feng, X.-G. Zhou, H.-F. Xiang and V. Roy, *Chem. Commun.*, 2012, **48**, 5139.

46 Z. A. Page, Y. Liu, V. V. Duzhko, T. P. Russell and T. Emrick, *Science*, 2014, **34**, 441.

47 R. Miyakoshi, K. Shimono, A. Yokoyama and T. Yokozawa, *J. Am. Chem. Soc.*, 2006, **128**, 16012.